International Journal of Heat and Mass Transfer xxx (2014) xxx–xxx

Contents lists available at ScienceDirect

International Journal of Heat and Mass Transfer

journal homepage: www.elsevier.com/locate/ijhmt

CFD analysis of power-law fluid flow and heat transfer around a confined semi-circular cylinder

Anuj Kumar [a], Amit Dhiman [a,1], László Baranyi [b,*]

[a] Department of Chemical Engineering, Indian Institute of Technology Roorkee, Roorkee 247 667, India
[b] Department of Fluid and Heat Engineering, Institute of Energy Engineering and Chemical Machinery, University of Miskolc, 3515 Miskolc-Egyetemváros, Hungary

ARTICLE INFO

Article history:
Received 11 September 2014
Received in revised form 11 November 2014
Accepted 11 November 2014
Available online xxxx

Keywords:
Semi-circular cylinder
Confined flow
Power-law index
Momentum transfer
Heat transfer
Drag coefficients and Nusselt number

ABSTRACT

A numerical analysis using Ansys Fluent was carried out to investigate the forced convection of power-law fluids (power-law index varying from 0.2 to 1.8) around a heated semi-circular cylinder with wall confinement (or blockage ratio) of 25%, Prandtl number of 50, and Reynolds numbers 1–40. Flow and thermal fields were found to be steady for Re up to 40. The shear-thickening behavior was found to have a higher value of drag coefficient, whereas the shear-thinning behavior had a smaller value of drag coefficient when compared with Newtonian fluids in the steady regime. The wake size was found shorter in shear-thickening fluids than Newtonian and shear-thinning fluids. An overall heat transfer rate was calculated and found to increase with the rise in Reynolds number. The average Nusselt numbers were observed higher for shear-thinning fluids than Newtonian and shear-thickening fluids; and the maximum enhancement in the heat transfer was achieved approximately 47% as compared to Newtonian fluids. The present results have also been correlated in terms of wake length, drag coefficient and average Nusselt number expressions for various Reynolds numbers and power-law indices studied. In addition, the effects of blockage ratios ranging from 16.67% to 50% on the engineering output parameters with varying power-law index at Re = 40 were reported.

1. Introduction

The viscous flow and heat transfer characteristics of a long semi-circular bluff body (or a semi-circular cylinder) not only have many practical applications like electronic cooling, pin type heat exchange systems, thermal processing of foodstuffs, papers, fibrous suspensions and others, but also offer space economy in terms of the specific heat transfer area. Also, under suitable settings of flow and heat transfer, most multiphase mixtures (foams, paper pulp suspensions, emulsions, fiber reinforced resin processing, etc.) and high molecular weight polymeric systems (solutions, blends, melts, etc.) exhibit shear-thinning and or shear-thickening behaviors [1–3]. Extensive literature suggests that many researchers have investigated numerically and or experimentally the non-Newtonian flow and heat transfer around bluff bodies like circular and square, but only a few corresponding details are available on momentum and heat transfer over a semi-circular cylinder in spite of its many engineering applications. The present work is concerned with the confined flow and heat transfer of power-law fluids around a semi-circular cylinder at low Reynolds numbers (Re) for the Prandtl number (Pr) of 50. The value of the Prandtl number of the order of 50 or so is very frequent in chemical, petroleum and oil related engineering applications and selected based on the widespread literature [4–6]. At the outset, it is appropriate to briefly review the relevant studies.

Significant investigations have been reported in the literature for Newtonian fluids around an unconfined semi-circular bluff body. Kiya and Arie [7] investigated numerically the fluid flow past semi-circular and semi-elliptical projections attached to a plane wall for Re ranging from 0.1 to 100. They reported geometrical shapes of front and rear standing vortices, drag coefficients, pressure and shear-stress distributions as functions of Re. Unlike [7], Forbes and Schwartz [8] examined the steady flow over a semi -circular obstacle on the bottom of a stream and the wave resistance was calculated at the free surface. In a similar study, Forbes [9] obtained the value of the critical flow by using upstream Froude number as a part of the solution in the formulation of Forbes and Schwartz [8] for the flow over a semi-circular obstruction. Experimentally, Boisaubert et al. [10] analyzed the flow over a semi-circular cylinder for flat and round sides facing the flow using a solid tracer visualization technique for Re = 60–600. They found

* Corresponding author. Tel.: +36 30 511 3834.
E-mail addresses: dhimuamit@rediffmail.com, amitdfch@iitr.ac.in (A. Dhiman), arambl@uni-miskolc.hu (L. Baranyi).
[1] Tel.: +91 1332 285890 (O), +91 9410329605 (M).

http://dx.doi.org/10.1016/j.ijheatmasstransfer.2014.11.046
0017-9310/© 2014 Published by Elsevier Ltd.

Nomenclature

C_D	total drag coefficient, dimensionless
C_{DF}	friction drag coefficient, dimensionless
C_{DP}	pressure drag coefficient, dimensionless
c_p	specific heat of the fluid, J kg^{-1} K^{-1}
C_p	Pressure coefficient, dimensionless
CV	control volume
D	diameter of a semi-circular cylinder, m
F_D	drag force per unit length of the obstacle, N m^{-1}
F_{DF}	friction drag force per unit length of the obstacle, N m^{-1}
F_{DP}	pressure drag force per unit length of the obstacle, N m^{-1}
h	local heat transfer coefficient, W m^{-2} K^{-1}
H	domain height, m
I_2	second invariant of the rate of the strain tensor, s^{-2}
k	thermal conductivity of the fluid, W m^{-1} K^{-1}
L	length of the domain, m
L_r/D	recirculation length, dimensionless
m	power-law consistency index, Pa s^n
n	power-law index, dimensionless
n_x	x-component of the direction vector normal to the surface of the cylinder, dimensionless
n_S	direction vector normal to the surface of the obstacle, dimensionless
Nu_L	local Nusselt number, dimensionless
Nu	average Nusselt number, dimensionless
p	Pressure, Pa
Pr	Prandtl number, dimensionless
Re	Reynolds number, dimensionless
S	arc length along the cross-section of a semi-circular cylinder
T	absolute temperature, K
T_∞	temperature of the fluid at the channel inlet, K
T_w	constant wall temperature at the surface of the cylinder, K
U_{avg}	average velocity of the fluid at the inlet, m s^{-1}
V_x, V_y	x- and y-components of the velocity, m s^{-1}
x, y	streamwise and transverse coordinates, m
X_d	downstream distance, m
X_u	upstream distance, m

Greek symbols

β	blockage ratio, d/H, dimensionless
δ	smallest size of the CV clustered around the obstacle, m
θ	dimensionless temperature, $(T - T_\infty)/(T_w - T_\infty)$
η	viscosity, Pa s
ρ	fluid density, kg m^{-3}
ε	component of rate of strain tensor, s^{-1}
τ	extra stress tensor, Pa

critical Reynolds numbers for the onset of vortex shedding as 140 and 190 for flat and curved surfaces, respectively. They also studied flow behavior by introducing a splitter plate behind the rounded body configuration and suggested the suitability of this arrangement as a flow-controlling device [11,12].

Kotake and Suwa [13] investigated the variation of stagnation points and the behavior of vortices in the rear of a semi-circular cylinder in the uniform shear flow by the visualization technique of the hydrogen bubble method. They showed that in case of shear flow, there was no vortex on the side with the faster main stream speed and the vortices were generated only on the slower speed side. Iguchi and Terauchi [14] studied the three kinds of non -circular cylinders (e.g. semi-circular, triangular and rectangular) to detect the shedding frequency of Karman's vortex streets for velocity lower than 10 cm/s. A triangular cylinder was found to meet the requirement most adequately as long as minimum detectable velocity was approximately 5 cm/s in the direction of flow approaching the triangular cylinder. Sophy et al. [15] examined the flow past a semi-circular cylinder with curved surface facing the flow and found the flow to be unsteady at Re = 65. They obtained the corresponding Strouhal number as 0.166, which was 7% larger than that of a circular cylinder at the corresponding transition. Coutanceau et al. [16] explained not only the way of formation of the initial wake vortices (primary and secondary vortices), but also their development with time behind a short cylindrical semi-circular shell. They reported about regime where structures changes occurred beyond the first phase of development when Re was between 120 and 140.

At high Re = 3500, Koide et al. [17] investigated the synchronization of Karman vortex shedding by giving a controlled cross-flow oscillation to circular, semi-circular and triangular cylinders. They showed that the synchronization region was almost the same for the three cylinders in spite of the different behaviors of separation point. Koide et al. [18] also experimentally investigated the influence of the cross-sectional configuration of a cylindrical body on Karman vortex excitation by using the same cylinders. They found that Karman vortex excitation appears on all the three cylinders, but the oscillation behavior was drastically different among them.

Recently, Chandra and Chhabra [19] reported the unconfined flow and heat transfer over a semi-circular cylinder immersed in Newtonian fluids for Re = 0.01–39.5 and Pr = 0.72–100. The critical Reynolds numbers for the wake formation and for the onset of vortex shedding were identified as 0.55–0.6 and 39.5–40, respectively. They showed that the total drag was dominated by the pressure contribution even at low Re. Similarly, the heat transfer results conform to the expected positive dependence on Re and Pr. Bhinder et al. [20] numerically investigated the forced convective heat transfer characteristics past a semi-circular cylinder at incidence for Re = 80–180 and Pr = 0.71. They showed that the increase in angle of incidence increases streamline curvature. Strouhal number showed a decreasing trend up to certain values of angle of attack and thereafter it increases marginally. A correlation of Strouhal number as a function of Re and angle of attack was established. In a similar study, Chatterjee et al. [21] simulated the forced convection heat transfer from a semi-circular cylinder in an unconfined flow regime for Re = 50–150 and Pr = 0.71. They considered two different configurations of the semi-circular cylinder; one when the curved surface facing the flow and the other when the flat surface facing the flow. They found significant differences in the global flow and heat transfer quantities for the two configurations studied, and concluded that the heat transfer rate was enhanced substantially when the curved surface was facing the flow rather than the flat surface. More recently, Sukesan and Dhiman [22] investigated the cross-buoyancy mixed convection around a confined semi-circular cylinder at low Re (1–40) for varying Pr (0.71–50) and blockage ratio (16.67–50%).

As far as the flow of non-Newtonian fluids around a semi-circular cylinder is concerned, Chandra and Chhabra [23] delineated the onset of flow separation from the surface of the unconfined semi-circular cylinder and the onset of the laminar vortex shedding regime for power-law fluids. They showed that irrespective of the type of fluid behavior (n = 0.2–1.8), both these transitions occur at the value of Re lower than that for a circular cylinder. Likewise, Chandra and

Chhabra [24] simulated the flow and heat transfer of power-law fluids over a semi-circular cylinder in the steady regime for the range of physical control parameters as Re = 0.01–30, Pr = 1–100 and n = 0.2–1.8. They showed that the heat transfer rate in shear-thinning (or pseudo-plastic) fluids (n < 1) can be enhanced by up to 60–70% under appropriate conditions, whereas shear-thickening (or dilatant) fluids (n > 1) slow down the heat transfer rate. Simple expressions for recirculation length, surface pressure and Nusselt number were also derived. They subsequently examined the effects of mixed [25] and natural [26,27] convection around a semi-circular cylinder to power-law fluids in the unconfined steady regime. In a recent study, Tiwari and Chhabra [28] investigated the flow of power-law fluids past a semi-circular cylinder with its flat face oriented upstream for Re = 0.01–25, n = 0.2–1.8 and Pr = 0.72–100. The critical Reynolds number for the onset of wake formation for a semi-circular cylinder with its curved face oriented in the upstream direction is found lower than that of a semi-circular cylinder with its flat face oriented in the upstream direction. In contrast, the critical Reynolds number for the onset of vortex shedding for a semi-circular cylinder with its curved face oriented in the upstream direction is found a little higher than that of a semi-circular cylinder with its flat face oriented in the upstream direction.

While the literature has dealt fairly extensively with momentum and heat transfer phenomena around a semi-circular cylinder for Newtonian fluids, studies dealing with non-Newtonian fluids are much rarer, and to the best of our knowledge, none have treated the case of a semi-circular cylinder in a channel, despite the many engineering applications [1–3]. Accordingly, the present work aims to fill this gap in the literature on the confined flow and heat transfer around a semi-circular cylinder at low Re for shear-thinning, Newtonian and shear-thickening behaviors.

2. Problem description

The channel confined flow was approximated by considering the laminar and incompressible flow (fully developed velocity profile) of power-law fluids across an infinitely long semi-circular cylinder (of diameter D) between the two parallel plane solid (adiabatic) walls, as shown schematically in Fig. 1. The power-law fluid at a temperature T_∞ at the inlet exchanges heat with the isothermal semi-circular cylinder whose surface was maintained at a temperature T_w such that $T_w > T_\infty$. The length and the height of the computational domain were identified as $L(=X_u + X_d)$ and H, respectively in axial and lateral dimensions. The semi-circular cylinder was located in the middle, i.e. at the center-line, at an upstream distance of X_u from the inlet and at a downstream distance of X_d from the outlet. It is worthwhile to mention that the output parameters such as drag coefficients and wake length with power-law fluids (n = 0.5–2) show an entirely different nature at high value of blockage (e.g. $\beta = D/H = 25\%$) at low Re (1–45) for the flow around a cylinder of square cross-section [29]. For instance, total drag coefficient always increases with increasing power-law index for β = 25% at a fixed Re; however, a mixed trend of increase or decrease with power-law index is reported for low blockages (β = 16.67% and 12.5%). Furthermore, Zdravkovich [30] reported for the flow around circular cylinders that for $0.1 < \beta < 0.6$ the blockage modifies the flow and the correction of data is necessary. However, this rough classification given in [30] is applicable for transition in shear layers, transition in boundary layers and fully turbulent states of flow. Therefore, the detailed flow and heat transfer investigations have been carried here at a blockage ratio of 25% based on the relevant studies in the confined domain [29–34].

The temperature difference between the surface of the semi-circular cylinder and the streaming liquid $(T_w - T_\infty)$ was kept low (=2 K) in this study so that the variation of the physical properties, notably density and viscosity with temperature could be neglected. Thus, the thermo-physical properties of the streaming liquid were assumed to be independent of the temperature. The viscous dissipation effects were also assumed to be negligible. The above-mentioned two assumptions restrict the applicability of these results to the situations for small temperature difference or where the temperature difference was not too significant and for moderate viscosity and or shearing levels.

The compact forms of continuity, momentum and energy equations for the present flow system are given below by Eqs. (1)–(3), respectively [2,3,35]:

$$\nabla \cdot \mathbf{V} = 0, \quad (1)$$

$$\rho(\mathbf{V} \cdot \nabla\mathbf{V} - \mathbf{f}) - \nabla \cdot \boldsymbol{\sigma} = 0, \quad (2)$$

$$\rho c_p(\mathbf{V} \cdot \nabla T) - k\nabla^2 T = 0. \quad (3)$$

Here $\mathbf{V}$ and $\mathbf{f}$ are defined as velocity (V_x and V_y were the components in Cartesian coordinates) and body force, respectively. The stress

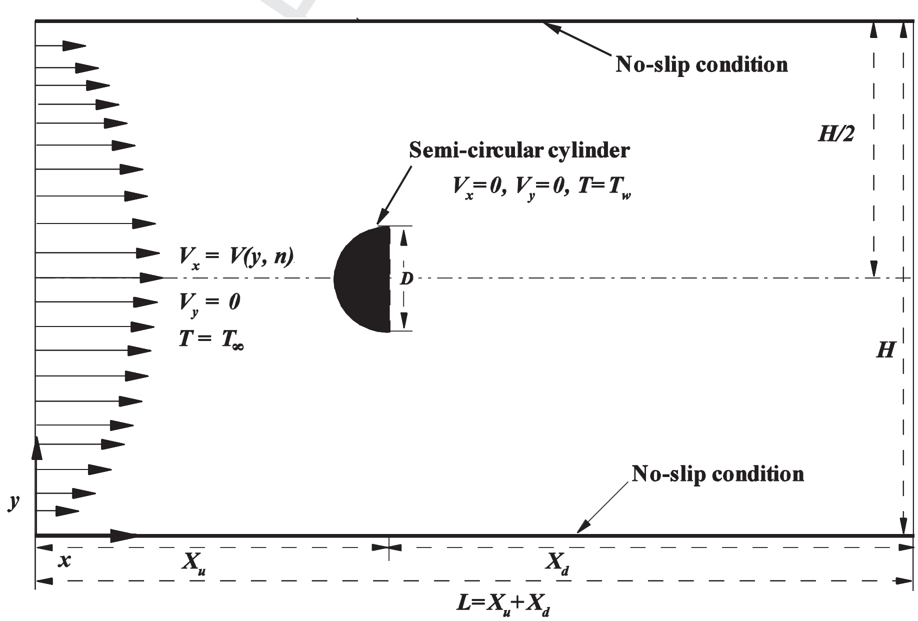

Fig. 1. Schematic of the confined flow and heat transfer in a channel with a built-in semi-circular cylinder.

tensor ($\boldsymbol{\sigma}$) was defined as the sum of the isotropic pressure (p) and the extra stress tensor ($\boldsymbol{\tau}$), i.e. $\boldsymbol{\sigma} = -p\mathbf{I} + \boldsymbol{\tau}$.

For incompressible fluids, the extra stress tensor was defined using viscosity (η) and component of the rate of strain tensor $\varepsilon(\mathbf{V})$ as

$$\boldsymbol{\tau} = 2\eta\varepsilon(\mathbf{V}), \tag{4}$$

where

$$\varepsilon(\mathbf{V}) = \frac{1}{2}\left[(\nabla\mathbf{V}) + (\nabla\mathbf{V})^T\right] \quad \text{and} \quad \eta = m\left(\frac{I_2}{2}\right)^{(n-1)/2}, \text{ where } I_2 = 2\left(\varepsilon_{xx}^2 + \varepsilon_{yy}^2 + \varepsilon_{xy}^2 + \varepsilon_{yx}^2\right).$$

The physical boundary conditions for the flow system under consideration can be written as follows:

- At inlet: a fully developed flow was assumed,

$$V_x = \left(\frac{2n+1}{n+1}\right)U_{avg}\left[1 - \left(\left|1 - \frac{2y}{H}\right|\right)^{(n+1)/n}\right] \text{ for } 0 \le y \le H, \; V_y = 0 \quad \text{and} \quad T = T_\infty. \tag{5}$$

- On top/bottom adiabatic channel wall: no-slip condition was applied,

$$V_x = 0, \; V_y = 0 \quad \text{and} \quad \frac{\partial T}{\partial y} = 0. \tag{6}$$

- On the semi-circular cylinder: no-slip condition was used,

$$V_x = 0, \; V_y = 0 \quad \text{and} \quad T = T_w. \tag{7}$$

- At outlet: it is located sufficiently far downstream from the semi-circular cylinder with a zero diffusion flux,

$$\frac{\partial V_x}{\partial x} = 0, \; \frac{\partial V_y}{\partial x} = 0 \quad \text{and} \quad \frac{\partial T}{\partial x} = 0. \tag{8}$$

The mathematical expressions of various engineering parameters utilized in this study are given as follows:

- Reynolds and Prandtl numbers for non-Newtonian power-law fluids were defined here as:

$$\mathrm{Re} = \frac{\rho D^n U_{avg}^{2-n}}{m} \quad \text{and} \quad \mathrm{Pr} = \frac{mc_p}{k}\left(\frac{U_{avg}}{D}\right)^{n-1}.$$

- Recirculation (or wake) length (L_r/D) was measured from the rear stagnation point to the point of reattachment for the near closed streamline on the line of symmetry in the downstream.
- Overall drag coefficient (C_D) and its components (C_{DP} and C_{DF}) were mathematically defined as:

$$C_D = \frac{F_D}{\frac{1}{2}\rho U_{avg}^2 D} = C_{DP} + C_{DF},$$

where

$$C_{DP} = \frac{F_{DP}}{\frac{1}{2}\rho U_{avg}^2 D} = \int_S C_p n_x dS \quad \text{and} \quad C_{DF} = \frac{F_{DF}}{\frac{1}{2}\rho U_{avg}^2 D} = \frac{2}{\mathrm{Re}}\int_S (\boldsymbol{\tau}\cdot n_S)dS.$$

- The local Nusselt number on the surfaces (curved and flat one) of the semi-circular cylinder was evaluated for the constant wall temperature as $\mathrm{Nu_L} = hD/k = -\partial\theta/\partial n_S$. These local values on each surface were then averaged to obtain the averaged Nusselt number of the semi-circular cylinder.

$$\mathrm{Nu} = \frac{1}{S}\int_S \mathrm{Nu_L}\, dS.$$

3. Numerical details

The numerical computations were carried out by solving the governing Eqs. (1)–(3) along with the boundary conditions (5)–(8) for the primitive variables, i.e. velocity (V_x and V_y), pressure (p) and temperature (T) fields by using a commercial computational fluid dynamics solver Ansys Fluent [36]. The two-dimensional, steady/unsteady, laminar, segregated solver was employed to solve the incompressible flow on the non-uniform collocated grid. The second-order upwind scheme was used to discretize convective terms, while the diffusive and the non-Newtonian terms were discretized by the central difference scheme. The SIMPLE scheme was used for solving pressure–velocity decoupling. The constant density and the non-Newtonian power-law viscosity model were used. The fully developed velocity profile at the channel inlet (see Eq. (5)) was incorporated by using the user-defined functions obtainable in Ansys Fluent [36]. Ansys Fluent solved the system of algebraic equations by using the Gauss–Siedel point-by-point iterative method in conjunction with the algebraic multi-grid method solver. The absolute convergence criteria of 10^{-10} for the continuity and x- and y-components of the velocity and of 10^{-15} for the energy were prescribed in the steady regime. In spite of this, the absolute convergence criteria of 10^{-15} each for the continuity, x- and y-components of the velocity and energy were used in the unsteady regime.

The computational grid was generated by using Gambit and its zoomed view around the semi-circular obstacle is shown in Fig. 2 for $\beta = 25\%$. A very fine grid of cell size (with number of control volumes (CVs) on the semi-circular cylinder equal to 340) of $0.01D$ was clustered around the semi-circular obstacle and near the channel walls; however, the largest grid size of $0.5D$ is utilized away from the semi-circular cylinder and channel walls.

The effect of the grid size on the dimensionless output parameters such as drag coefficient (C_D) and average Nusselt number (Nu) was investigated at three grid structures (symbolically represented as G1, G2 and G3 with 250, 340 and 400 CVs prescribed on the surfaces of a semi-circular cylinder) for $\mathrm{Re} = 40$, $\mathrm{Pr} = 50$, $\beta = 25\%$ and $n = 0.2$, 1, 1.8 (Table 1). The relative percent differences in the values of C_D and Nu for the grid G1 (250 CVs) with respect to the values at the grid G3 (400 CVs) for $n = 0.2$ were found to be about 3% and 2%, respectively. For $n = 1$, the relative percent differences in the values of C_D and Nu for the grid G1 (250 CVs) with respect to the values at the grid G3 (400 CVs) were found to be about 2.2% and 2.5%, respectively. Similarly, at $n = 1.8$, the relative differences in the values of C_D and Nu for the grid G1 (250 CVs) with respect to the values at the grid G3 (400 CVs) were found to be about 1.3% and 3%, respectively. On the other hand, the corresponding differences in the values of C_D and Nu for the grid G2 (340 CVs) with respect to the values at the finest grid G3 (400 CVs) were found to be only 1% and less than 1.1%, respectively. Thus, the grid G2 was used to generate further results.

The domain dependence study was conducted to determine the effects of upstream (Table 2) and downstream (Table 3) distances on the dimensionless output parameters as follows. The influence of the upstream distance for $\beta = 16.67\%$ on the values of physical parameters was investigated for $X_u = 30D, 45D$ and $60D$ for $\mathrm{Re} = 40$ and $\mathrm{Pr} = 50$ at $n = 0.2$, 1 and 1.8 (Table 2). For $n = 0.2$, 1 and 1.8, the relative percent differences in the values of C_D and Nu for $X_u/D = 45$ with respect to $X_u/D = 60$ were found to be less than 1% for both C_D and Nu. Similarly, the influence of the downstream distance on the values of physical parameters was investigated for $X_d = 100D, 120D$ and $140D$ for the same values of Re, Pr and n (Table 3). The relative percent differences were found to be less than 0.6% for both C_D and Nu for $X_d/D = 120$ with respect to $X_d/D = 140$. For $\beta = 25\%$, the relative percent differences in the

Please cite this article in press as: A. Kumar et al., CFD analysis of power-law fluid flow and heat transfer around a confined semi-circular cylinder, Int. J. Heat Mass Transfer (2014), http://dx.doi.org/10.1016/j.ijheatmasstransfer.2014.11.046

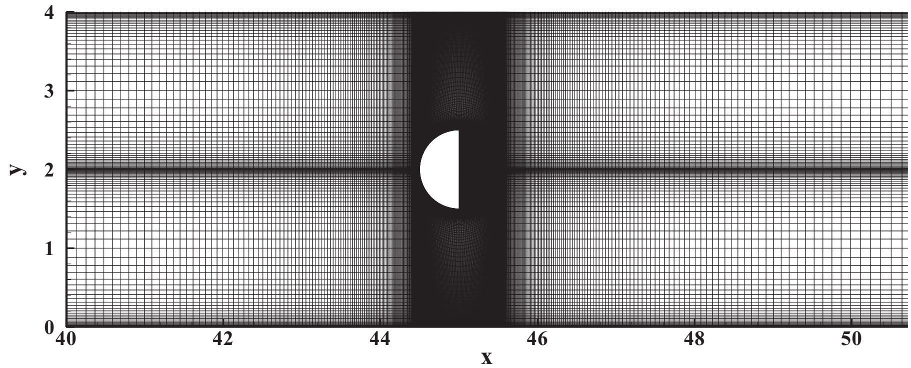

Fig. 2. Magnified view of the grid around a semi-circular cylinder for $\beta = 25\%$.

Table 1
Grid dependence study for Re = 40, n = 0.2, 1, 1.8 and Pr = 50.

Grid details				C_D			Nu		
	δ/D	CVs on semi-circular cylinder	Total number of cells in domain	n					
				0.2	1	1.8	0.2	1	1.8
G1	0.1	250	43436	1.961	4.088	6.457	25.997	18.880	15.552
G2	0.01	340	103579	1.905	4.001	6.650	26.588	19.154	15.852
G3	0.008	400	127691	1.905	4.000	6.649	26.597	19.379	16.028

Table 2
Effect of upstream distance on the dimensionless output parameters for Re = 40 and Pr = 50 at different values of β and n.

X_u/D	C_D			Nu		
	n					
	0.2	1	1.8	0.2	1	1.8
$\beta = 16.67\%$						
30	1.655	3.336	5.047	24.796	18.482	15.276
45	1.653	3.336	5.047	24.776	18.491	15.274
60	1.637	3.335	5.047	24.647	18.51222	15.271
$\beta = 25\%$						
30	1.887	4.002	6.630	26.605	19.160	15.852
45	1.905	4.001	6.650	26.588	19.154	15.851
60	1.915	4.002	6.650	26.361	19.138	15.847
$\beta = 50\%$						
30	3.762	9.329	36.611	31.220	22.215	16.445
45	3.747	9.321	36.572	31.469	22.283	16.467
60	3.726	9.319	36.110	31.554	22.418	16.474

Table 3
Effect of downstream distance on the dimensionless output parameters for Re = 40 and Pr = 50 at different values of β and n.

X_d/D	C_D			Nu		
	n					
	0.2	1	1.8	0.2	1	1.8
$\beta = 16.67\%$						
100	1.652	3.336	5.047	24.710	18.410	15.289
120	1.653	3.336	5.047	24.776	18.491	15.274
140	1.656	3.332	5.047	24.901	18.502	15.291
$\beta = 25\%$						
100	1.879	4.002	6.647	26.606	19.140	15.868
120	1.905	4.002	6.650	26.588	19.154	15.851
140	1.914	4.001	6.645	26.572	19.169	15.848
$\beta = 50\%$						
100	3.727	9.319	36.421	31.579	22.310	16.593
120	3.747	9.321	36.572	31.469	22.283	16.467
140	3.751	9.319	36.624	31.239	22.110	16.450

values of C_D and Nu for $X_u/D = 45$ were found to be less than 0.9% with respect to the values at $X_u/D = 60$ for n = 0.2, 1, and 1.8 (Table 2). Whereas, the corresponding differences in the downstream distances for $X_d/D = 120$ were found to be less than 0.5% for both the output parameters with respect to $X_d/D = 140$ (Table 3). Along the same line, for $\beta = 50\%$, the relative differences in the values of both C_D and Nu for $X_u/D = 45$ were found to be less than 1.3% of the corresponding values at $X_u/D = 60$, whereas the corresponding differences in the downstream distances for $X_d/D = 120$ were found to be less than 0.8% with respect to $X_d/D = 140$ for both the output parameters (Table 3). Thus, the dimensionless upstream and downstream distances of 45 and 120 were found adequate for the present results to be free from end effects.

4. Results and discussion

The confined flow of power-law fluids ($0.2 \leq n \leq 1.8$) was simulated here for Re = 1–40 and for the fixed blockage ratio of 25% [31–34] at the Prandtl number of 50 [4–6]. Additionally, the effects of blockage ratios of 16.67%, 25%, and 50% on the engineering output parameters with varying power-law index at the maximum value of Reynolds number investigated here (Re = 40) were reported. It is to be noted that Chandra and Chhabra [19] found the transition from a steady to a time-periodic regime between Re = 39.5 and 40 for the flow around a semi-circular cylinder in the unconfined domain. Therefore, time-dependent computations have also been carried out for the present confined flow configuration with a built-in semi-circular cylinder at Re = 40 for the extreme values of blockage ratios (16.67% and 50%) and power-law indices (0.2 and 1.8) studied. The flow and the thermal fields were found to be steady for the entire range of settings covered in this study. This is attributed to the fact that as the blockage increases the flow tends to stabilize, because the walls are nearer to the semi-circular cylinder.

Unfortunately no literature is available for the confined flow of power-law fluids across a semi-circular cylinder, so the bench-

Please cite this article in press as: A. Kumar et al., CFD analysis of power-law fluid flow and heat transfer around a confined semi-circular cylinder, Int. J. Heat Mass Transfer (2014), http://dx.doi.org/10.1016/j.ijheatmasstransfer.2014.11.046

marking of the present numerical solution procedure was made for the unconfined case in the steady regime for n = 0.2–1.8 and Re = 1–30 by using the identical computational domain of Chandra and Chhabra [25]. Excellent agreement can be seen between the present results and the values reported in [25] (Table 4). For instance, the maximum differences in the values of total drag coefficients and average Nusselt numbers were found to be less than 1.3% and about 1.6%, respectively. Additional benchmarking of the numerical methodology employed can be found in our recent study for the confined power-law flow and heat transfer around an inclined square bluff body [6].

4.1. Flow and thermal patterns

Flow structures in the vicinity of the long semi-circular obstacle were shown by streamline contours at the blockage ratio of 25% for the extreme and the intermediate values of Re (1, 20 and 40) and n (0.2, 1 and 1.8) in Fig. 3a–i. The streamline contours showed a condition of no flow separation from the surface of the semi-circular cylinder at Re = 1 for the entire range of n studied, due to the dominant viscous force at this low value of Re. The flow separation occurred on increasing the value of Re (>1) from the rear or the flat surface of the semi-circular cylinder. Two standing symmetric vortices, rotating in opposite directions, were observed behind the semi-circular obstacle in the steady regime, as can be seen in Fig. 3. As expected, the size of these vortices increases with an increase in Re for the constant value of n. But the size of these vortices was found to decrease as the fluid behavior changed from shear-thinning to shear-thickening for the constant Re. These findings were consistent with the power-law studies reported on the confined circular [31,37] and square [5,29] cylinders in the steady regime.

Thermal patterns provide knowledge of the detailed temperature field around an obstacle, which can be significant in the designing of a variety of heat exchange systems particularly in the processing of temperature sensitive materials such as foodstuffs, personal care products and others. Fig. 4a–i display the representative isotherm contours around the semi-circular cylinder in the steady regime at Pr = 50. As expected, the curved (or upstream) surface of the semi-circular cylinder had the maximum clustering of isotherms and the minimum on the flat (or downstream) surface. As a result, higher rate of heat transfer was observed from the curved surface than the flat one. The increased value of Re for the constant value of n resulted in the increase in the temperature gradient around the obstacle due to the thinning of momentum and thermal boundary layers and increase in circulation of large amount of fluid, thus an increase in the heat transfer rate was observed. These findings were consistent with the power-law studies reported on the confined heated circular [38] and square [5,39] cylinders in a channel at low Re. On the other hand, decomposing of steady temperature fields was observed with the increase in shear-thickening behavior for the fixed value of Re; however, these effects were more prominent at the high value of Re. Thus, the heat transfer rate was enhanced by the increase in n for the fixed Re. The trends observed here were strongly dependent on the value of Re.

4.2. Wake length

The phenomenon of flow recirculation in the rear of the obstacle was often visualized in terms of the recirculation (or wake) length. Fig. 5 displays the dependence of the recirculation length (L_r/D) on Re and n at the blockage ratio of 25%. No flow separation was observed at Re = 1 (i.e. the wake length is zero here) for any value of n studied (Figs. 3 and 5), but at Re = 5 the separation of boundary layer was observed for all values of n. As expected, the wake region increased with the increase in Re for the fixed value of n. The length of the recirculation zone increased when moving from shear-thickening to shear-thinning nature (or when decreasing the value of n) for the fixed value of Re. These findings were consistent with the power-law studies available on the steady flow around confined circular [37] and square [5,29] cylinders.

The present wake length results further can be approximated somewhat better by the following expression for the settings $1 < \mathrm{Re} \leqslant 40$ and $0.2 \leqslant n \leqslant 1.8$ at $\beta = 25\%$,

$$L_r/D = \mathrm{Re}^{[1.2+0.0315(\ln(n))^2]} \exp[(-2.8405 - 0.1212n^3) - (0.0142n^{-0.0502})\mathrm{Re}]. \quad (9)$$

Eq. (9) has the average deviation of about 5.5% and the maximum deviation of less than 10%, when compared with the present computed results.

4.3. Overall drag coefficient and its components

Fig. 6a shows the dependence of the pressure drag coefficient (C_{DP}) for a semi-circular cylinder on Re and n at β = 25%. For a fixed value of Re, the value of the pressure drag coefficient decreased as the fluid behavior changes from shear-thickening to shear -thinning. The influence of n was found more prominent at low Re and its effect on the pressure drag gradually diminished as Re

Table 4
Comparison of present drag and Nusselt number results for the flow around a semi-circular cylinder with literature [25] at various values of Re and n in the unconfined domain.

Re	n	Present work		Chandra and Chhabra [25]	
		C_D	Nu	C_D	Nu
1	0.2	26.216	4.613	26.020	4.646
	1	10.050	2.798	10.170	2.836
	1.8	5.730	2.675	5.782	2.665
5	0.2	5.585	8.829	5.611	8.975
	1	3.882	5.397	3.854	5.471
	1.8	3.149	4.897	3.189	4.952
10	0.2	3.078	12.645	3.104	12.771
	1	2.710	7.465	2.721	7.577
	1.8	2.529	6.829	2.541	6.893
30	0.2	1.428	23.069	1.432	23.065
	1	1.690	13.581	1.696	13.752
	1.8	1.805	11.948	1.817	11.882

Please cite this article in press as: A. Kumar et al., CFD analysis of power-law fluid flow and heat transfer around a confined semi-circular cylinder, Int. J. Heat Mass Transfer (2014), http://dx.doi.org/10.1016/j.ijheatmasstransfer.2014.11.046

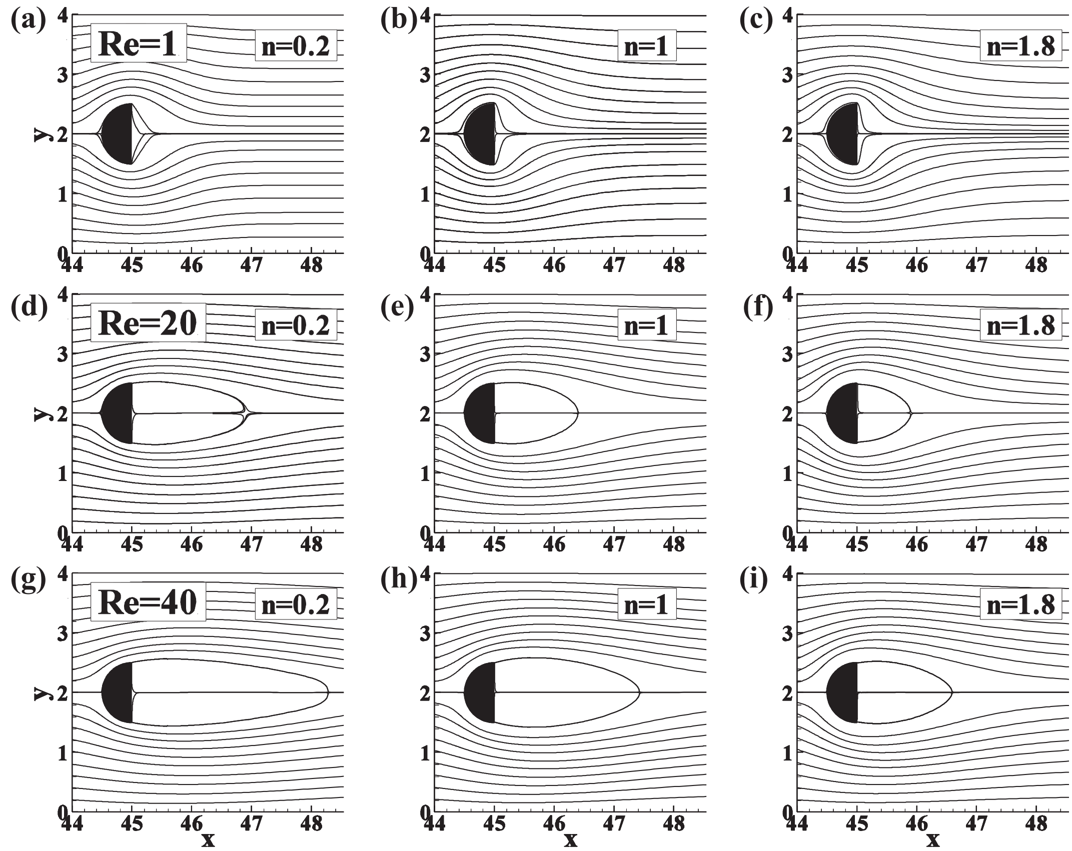

Fig. 3. Streamlines for Re = 1, 20 and 40 for n = 0.2, 1 and 1.8 in the steady regime for β = 25%.

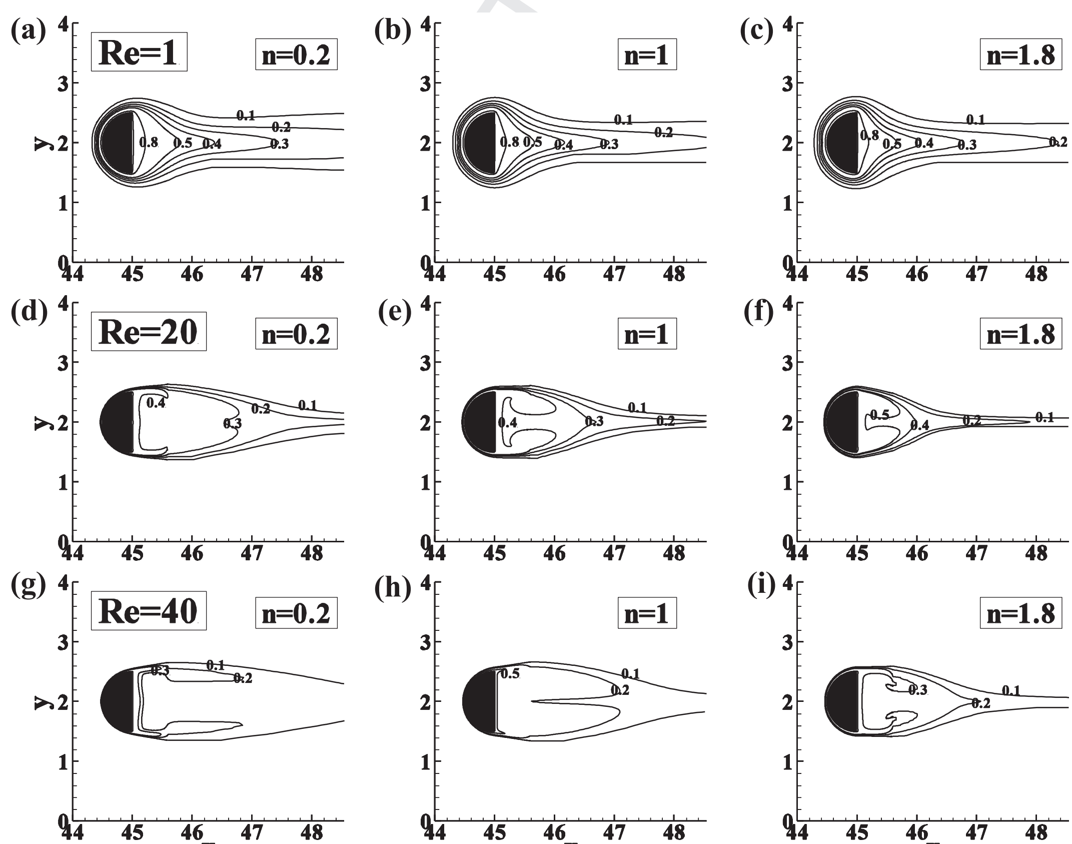

Fig. 4. Isotherm contours for Re = 1, 20 and 40 for n = 0.2, 1 and 1.8 in the steady regime for β = 25%.

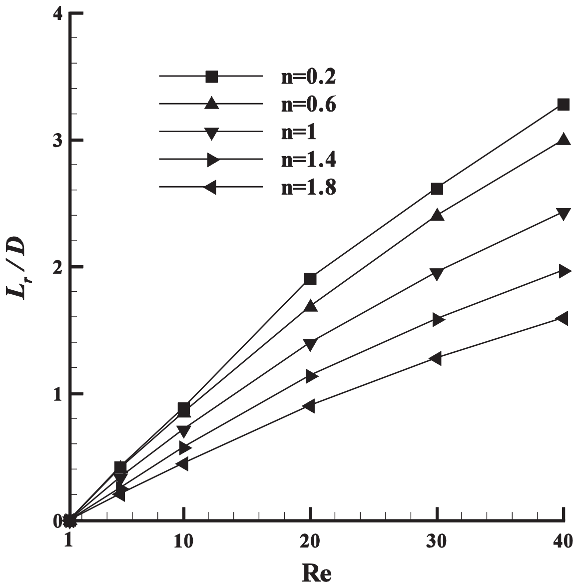

Fig. 5. Variation of wake length (L_r/D) with Re at different values of n in the steady regime for $\beta = 25\%$.

was increased, a similar trend was seen for spheroid and spherical particles [1,2] where inertial forces overshadowed the viscous forces with increasing Re, hence independent of the type of fluid (shear-thinning, shear-thickening and Newtonian). Similarly, at a fixed value of Re, the dependence of the friction drag coefficient (C_{DF}) was increased with increasing n as the viscous force increases with increasing n (Fig. 6b). When Re was gradually increased, the dependence of the friction drag coefficient on n decreases. Broadly, the larger the Re the weaker the dependence on n. These trends were clearly due to the non-linear nature of the viscosity over the surface of the semi-circular cylinder [24]. The viscosity for the shear-thickening fluids becomes very large as the shear rate decreases and hence it tends to infinity far-away from the semi-circular cylinder. Therefore, the viscous effects dominate far-away from the semi-circular cylinder. Along the same line, the dependence of the total drag coefficient(C_D) on n was seen to be stronger at low values of Re, thus a significant variation in the drag values could be seen in shear-thickening, Newtonian and shear-thinning fluids (Fig. 6c). The value of C_D increased when n increases from 0.2 to 1.8. These trends were qualitatively consistent with the literature values for the unconfined power-law flow past a semi-circular cylinder in the steady regime [24]. The total drag coefficient over the entire range of Re and n studied can be represented by the following correlation:

$$C_D = 0.7445 + 2.1n - 0.1503n^3 + (4.7196 + 18.3703 \times \exp(n))/\mathrm{Re} + (3.0881 - 15.8919n^2 + 3.84n^3) \times \ln(\mathrm{Re})/\mathrm{Re}^2. \quad (10)$$

Eq. (10) has an average deviation of less than 1% and the maximum deviation of about 3.2% with the present computed results.

Further examination of the present results in terms of the variation of the drag ratio (C_{DP}/C_{DF}) on Re and n at $\beta = 25\%$ reveals that this ratio decreases with the increase in n for the range of parameters studied in this work (Fig. 6d). Qualitatively, this effect can be explained as follows: for a fixed value of Re, the viscous forces scale as U^n_{avg}. For a shear-thickening fluid, as the value of n is gradually increased, the viscous forces increase. Similarly, for a shear-thinning fluid, viscous forces increased more steeply. In either case, the C_{DP}/C_{DF} ratio decreased with n, as shown in Fig. 6d. A rapid

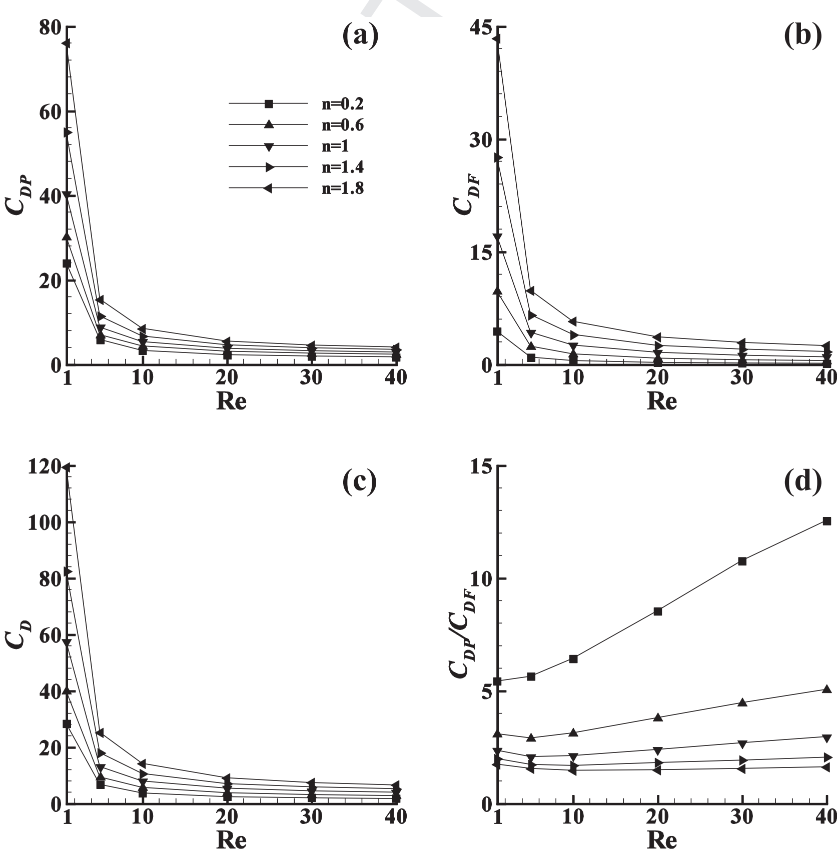

Fig. 6. (a–c) Variation of individual and total drag coefficients (C_{DP}, C_{DF}, C_D) and (d) drag ratio (C_{DP}/C_{DF}) with Re and n in the steady regime for $\beta = 25\%$.

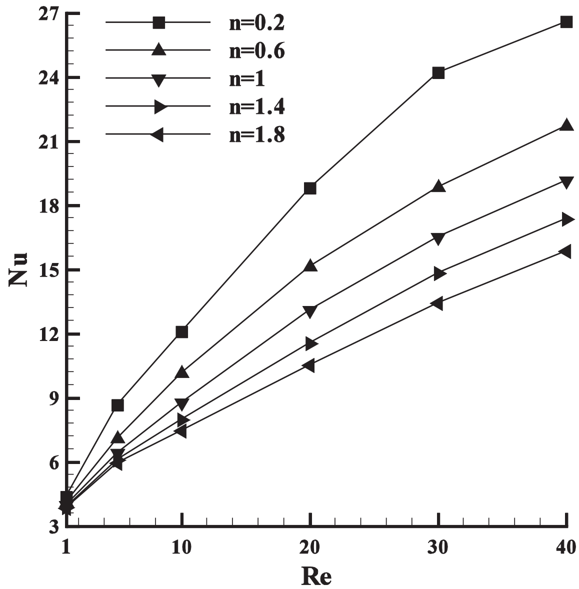

Fig. 7. Variation of the average Nusselt number as a function of Re and n at Pr = 50 in the steady regime for β = 25%.

decrease in the drag ratio with an increase in n was seen at low Re in shear-thickening fluids, i.e. strong dependence on n.

4.4. Average Nusselt number

The variation of the average Nusselt number (Nu) for the varying values of Re and n for the value of Prandtl number at β = 25% is depicted in Fig. 7. It can be seen that the heat transfer rate increased with the increase in the value of Re for the constant value of n. Similarly, as the value of n was increased, for the constant value of Re, the average Nusselt number decreases. The average Nusselt number is found higher for shear-thinning fluids than Newtonian and shear-thickening fluids. The maximum enhancement in the heat transfer is found approximately 47% for shear-thinning fluid (for Re = 30 and n = 0.2) with respect to Newtonian behavior. It is also found that the value of the heat transfer in the confined semi-circular cylinder is always greater than that of the unconfined semi-circular cylinder for power-law fluids in the steady regime [24].

Furthermore, the following simple expressions have been developed to represent the average cylinder Nusselt number as the function of Re and n. After a thorough study, it was observed that two different average Nusselt number expressions, namely Eq. (11) for $0.2 \leqslant n \leqslant 1$ and Eq. (12) for $1 < n \leqslant 1.8$, can be used such that their maximum deviations with the computed results for the entire range of Re covered at β = 25% were less than 5%:

$$\mathrm{Nu} = (3.3704n/(0.01 + n)) + (1.581/(1 + 1.232n))\,\mathrm{Re} - (0.13 \times 0.3744^{n})\mathrm{Re}^{1.5}, \quad (11)$$

$$\mathrm{Nu} = 3.9337 - 0.03095n + (-0.1737n + 0.8224)\,\mathrm{Re}^{0.5}\ln(\mathrm{Re}). \quad (12)$$

Expression (11) has the maximum deviation of less than 3.6%, with the present computed results and the corresponding average deviation is of less than 1.2%. Similarly, Eq. (12) has the maximum and the average deviations of less than 3.9% and less than 1.3%, respectively, with the present computed results.

4.5. Effect of blockage ratio

To present the influence of blockage ratio on the engineering output parameters, Fig. 8a–d depict the variation of individual

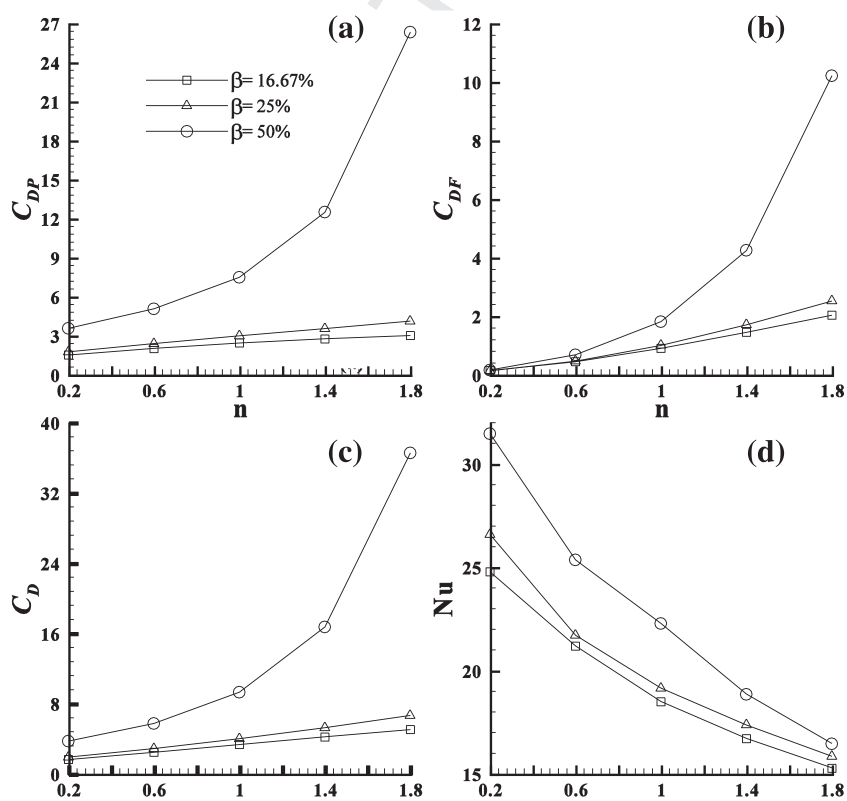

Fig. 8. (a–c) Variation of individual and total drag coefficients (C_{DP}, C_{DF}, C_D) and (d) average cylinder Nusselt number (Nu) for n = 0.2–1.8 and β = 16.67%, 25%, and 50% at Re = 40 and Pr = 50.

and overall drag coefficients and average cylinder Nusselt number as a function of power-law index for β = 16.67–50% at Re = 40 and Pr = 50.

The drag coefficients were found to increase with increasing blockage ratio for the fixed value of the power-law index. Similarly, the drag coefficients increased with increasing power-law index for the fixed blockage ratio. The values of drag coefficients were found most affected between blockages of 25% and 50%, but a small corresponding change in the values of drag coefficients was observed between the blockages of 25% and 16.67%. For instance, a quite a big change of approximately 550% (at n = 1.8) was observed in the values of overall drag coefficients for β = 50% with respect to the corresponding values at β = 25%. However, a small change in the values of overall drag coefficients of approximately 32% (at n = 1.8) was observed for β = 25% with respect to the corresponding values at β = 16.67%. The drag ratio (as defined in Section 4.3) was observed to decrease sharply with increasing power-law index; however, it increased with increasing blockage ratio. In other words, the contribution of the pressure drag coefficient to the overall drag coefficient was always found more than that of the friction drag coefficient for the range of settings studied.

Similar to the drag coefficients, the rate of heat transfer was found to increase with increasing wall confinement for the constant value of n because of the increase in the thermal gradients. However, as opposed to the drag coefficients, the average cylinder Nusselt number was found to increase as the value of power-law index decreased from 1.8 to 0.2 (or as the shear-thinning tendency increased) for the constant blockage ratio. The maximum enhancement in heat transfer for the highest blockage ratio of 50% with respect to the lowest blockage ratio of 16.67% used was found to be approximately 27% at n = 0.2.

5. Conclusions

Effects of power-law fluids in a channel with a built-in long heated semi-circular cylinder were investigated for the various values of Re (1–40) and n (0.2–1.8) at the values of blockage ratio of 25% and Prandtl number of 50. Extensive numerical computations free from domain and mesh size effects were performed to calculate wake length, drag coefficients and average Nusselt number. For a fixed value of Re, the length of the recirculation zone decreased with an increase in the value of n. Drag coefficients were found to increase with the increase in the value of n for the fixed Re. Also, the values of individual and total drag coefficients showed the usual inverse dependence on Re for the fixed value of n. As is well known, the heat transfer rate increased with the increase in Re for the constant value of n. Similarly, when the value of n increased the average Nusselt number decreased. The maximum enhancement in heat transfer for shear-thinning fluids was found approximately 47% with respect to Newtonian behavior at β = 25%. The correlations of wake length, overall drag coefficient and average Nusselt number were also established. Finally, the effect of blockage ratio (16.67–50%) on the flow and heat transfer output parameters was investigated for the varying power-law indices (0.2–1.8) at the fixed values of Re = 40 and Pr = 50. The drag coefficients and the average cylinder Nusselt number increased with increasing blockage ratio for any value of n. The drag coefficients were found to increase with increasing n, whereas the average cylinder Nusselt number increased as the value of n decreased. Flow and thermal fields were found to be steady for the entire range of parameters investigated. A more detailed investigation of the effects of blockage ratios on the flow and heat transfer characteristics at different Prandtl numbers would be the scope for future research.

Conflict of interest

None declared.

Acknowledgments

The third author gratefully acknowledges the support of the TÁMOP-4.2.1.B-10/2/KONV-2010-0001 project in the framework of the New Hungarian Development Plan. The realization of this project is supported by the European Union, co-financed by the European Social Fund.

The authors also would like to thank the two anonymous reviewers for their valuable and helpful comments on this work.

References

[1] R.P. Chhabra, Hydrodynamics of non-spherical particles in non-Newtonian fluids, in: N.P. Cheremisinoff, P.N. Cheremisinoff (Eds.), Handbook of Applied Polymer Processing Technology, Marcel Dekker, New York, 1996. Chapter 1.
[2] R.P. Chhabra, Bubbles, Drops and Particles in Non-Newtonian Fluids, second ed., CRC Press, Boca Raton, FL, 2006.
[3] R.P. Chhabra, Fluid flow and heat transfer from circular and non-circular cylinders submerged in non-Newtonian liquids, Adv. Heat Transfer 43 (2011) 289–417.
[4] M. Bouaziz, S. Kessentini, S. Turki, Numerical prediction of flow and heat transfer of power-law fluids in a plane channel with a built-in heated square cylinder, Int. J. Heat Mass Transfer 53 (2010) 5420–5429.
[5] N. Sharma, A. Dhiman, S. Kumar, Non-Newtonian power-law fluid flow around a heated square bluff body in a vertical channel under aiding buoyancy, Numer. Heat Transfer A 64 (2013) 777–799.
[6] A. Kumar, A.K. Dhiman, R.P. Bharti, Power-law flow and heat transfer over an inclined square bluff body: effect of blockage ratio, Heat Transfer-Asian Res. 43 (2014) 167–196.
[7] M. Kiya, M. Arie, Viscous shear flow past small bluff bodies attached to a plane wall, J. Fluid Mech. 69 (1975) 803–823.
[8] L.K. Forbes, L.W. Schwartz, Free-surface flow over a semi-circular obstruction, J. Fluid Mech. 114 (1982) 299–314.
[9] L.K. Forbes, Critical free surface flow over a semi-circular obstruction, J. Eng. Math. 22 (1988) 3–13.
[10] N. Boisaubert, M. Coutanceau, P. Ehrmann, Comparative early development of wake vortices behind a short semicircular-section cylinder in two opposite arrangements, J. Fluid Mech. 327 (1996) 73–99.
[11] N. Boisaubert, M. Coutanceau, A. Texier, Manipulation of the starting semicircular cylinder near-wake by means of a splitter plate, J. Flow Visual. Image Process. 4 (1997) 211–221.
[12] N. Boisaubert, A. Texier, Effect of splitter plate on the near-wake development of a semicircular cylinder, Exp. Therm. Fluid Sci. 16 (1998) 100–111.
[13] M. Kotake, S. Suwa, Flow visualization around a semi circular cylinder in a uniform shear flow, J. Visual. Soc. Jpn. 21 (2001) 95–98.
[14] M. Iguchi, Y. Terauchi, Karman vortex probe for the detection of molten metal surface flow in low velocity range, ISIJ Int. 42 (2002) 939–943.
[15] T. Sophy, H. Sada, D. Bouard, Calcul de l'ecoulementautour d'un cylindre semi-circulaire par une method de collocation, C.R. Mecanique 330 (2002) 193–198.
[16] M. Coutanceau, C. Migeon, P. Ehrmann, Particulars of the cross and spanwise near-wake development of a short semicircular-section shell, through the transition Re-range (60 < Re < 600), J. Visual. 3 (2000) 9–26.
[17] M. Koide, S. Tomida, T. Takahashi, L. Baranyi, M. Shirakashi, Influence of cross-sectional configuration on the synchronization of Karman vortex shedding with the cylinder oscillation, JSME Int J., Ser. B 45 (2002) 249–258.
[18] M. Koide, T. Takahashi, M. Shirakashi, Influence of cross-sectional configuration on Karman vortex excitation, J. Comp. Appl. Mech. 5 (2004) 297–310.
[19] A. Chandra, R.P. Chhabra, Flow over and forced convection heat transfer in Newtonian fluids from a semi-circular cylinder, Int. J. Heat Mass Transfer 54 (2011) 225–241.
[20] A.P.S. Bhinder, S. Sarkar, A. Dalal, Flow over and forced convection heat transfer around a semi-circular cylinder at incidence, Int. J. Heat Mass Transfer 55 (2012) 5171–5184.
[21] D. Chatterjee, B. Mondal, P. Halder, Unsteady forced convection heat transfer over a semi-circular cylinder at low Reynolds numbers, Numer. Heat Transfer A 63 (2013) 411–429.
[22] M.K. Sukesan, A.K. Dhiman, Laminar mixed convection in a channel with a built-in semi-circular cylinder under the effect of cross-buoyancy, Int. Commun. Heat Mass Transfer 58 (2014) 25–32.
[23] A. Chandra, R.P. Chhabra, Influence of power-law index on transitional Reynolds numbers for flow over a semi-circular cylinder, Appl. Math. Model. 35 (2011) 5766–5785.
[24] A. Chandra, R.P. Chhabra, Momentum and heat transfer characteristics of a semi-circular cylinder immersed in power-law fluids in the steady flow regime, Int. J. Heat Mass Transfer 54 (2011) 2734–2750.

Please cite this article in press as: A. Kumar et al., CFD analysis of power-law fluid flow and heat transfer around a confined semi-circular cylinder, Int. J. Heat Mass Transfer (2014), http://dx.doi.org/10.1016/j.ijheatmasstransfer.2014.11.046

[25] A. Chandra, R.P. Chhabra, Mixed convection from a heated semi-circular cylinder to power-law fluids in the steady flow regime, Int. J. Heat Mass Transfer 55 (2012) 214–234.
[26] A. Chandra, R.P. Chhabra, Laminar free convection from a horizontal semi-circular cylinder to power-law fluids, Int. J. Heat Mass Transfer 55 (2012) 2934–2944.
[27] A.K. Tiwari, R.P. Chhabra, Laminar natural convection in power-law liquids from a heated semi-circular cylinder with its flat side oriented downward, Int. J. Heat Mass Transfer 58 (2013) 553–567.
[28] A.K. Tiwari, R.P. Chhabra, Momentum and heat transfer characteristics for the flow of power-law fluids over a semicircular cylinder, Numer. Heat Transfer A 66 (2014) 1365–1388.
[29] A.K. Dhiman, R.P. Chhabra, V. Eswaran, Steady flow across a confined square cylinder: effects of power-law index and of blockage ratio, J. Non-Newtonian Fluid Mech. 148 (2008) 141–150.
[30] M.M. Zdravkovich, Flow Around Circular Cylinders: Applications, vol. 2, Oxford University Press, New York, 2003.
[31] S. Bijjam, A.K. Dhiman, CFD analysis of two-dimensional non-Newtonian power-law flow across a circular cylinder confined in a channel, Chem. Eng. Commun. 199 (2012) 767–785.
[32] H. Abbassi, S. Turki, S.B. Nasrallah, Numerical investigation of forced convection in a plane channel with a built-in triangular prism, Int. J. Therm. Sci. 40 (2001) 649–658.
[33] S. Srikanth, A.K. Dhiman, S. Bijjam, Confined flow and heat transfer across a triangular cylinder in a channel, Int. J. Therm. Sci. 49 (2010) 2191–2200.
[34] R. Agarwal, A. Dhiman, Flow and heat transfer phenomena across two confined tandem heated triangular bluff bodies, Numer. Heat Transfer A 66 (2014) 1020–1047.
[35] R.B. Bird, W.E. Stewart, E.N. Lightfoot, Transport Phenomena, second ed., Wiley, New York, 2002.
[36] ANSYS User Manual, Ansys, Inc., Canonsburg, PA, 2009.
[37] R.P. Bharti, R.P. Chhabra, V. Eswaran, Two-dimensional steady Poiseuille flow of power-law fluids across a circular cylinder in a plane confined channel: wall effects and drag coefficients, Ind. Eng. Chem. Res. 46 (2007) 3820–3840.
[38] R.P. Bharti, R.P. Chhabra, V. Eswaran, Effect of blockage on heat transfer from a cylinder to power-law liquids, Chem. Eng. Sci. 62 (2007) 4729–4741.
[39] A.K. Dhiman, Heat transfer to power-law dilatant fluids in a channel with a built-in square cylinder, Int. J. Therm. Sci. 48 (2009) 1552–1563.